Brazilian Journal of Physics (2022) 52:207
https://doi.org/10.1007/s13538-022-01206-4

SOCIEDADE BRASILEIRA DE FÍSICA

CONDENSED MATTER

Structural and Compositional Analyses of Spray Pyrolysis α-Lanthanum Sulphide (α-La_2S_3) Thin Films

Sabrina Tair[1] · Abdelkader Nebatti Ech-Chergui[1,9] · Sanat Kumar Mukherjee[3] · Abdelwaheb Boukhachem[4] · Rajan Kr. Singh[3] · Noureddine Benaioun[2] · M'hamed Guezzoul[5] · Mohammed Reda Chellali[6] · Abdelhalim Zoukel[7] · Fares Boussahoul[8] · Kouider Driss-Khodja[2] · Bouhalouane Amrani[2]

Received: 24 March 2022 / Accepted: 30 September 2022 / Published online: 20 October 2022

Abstract
This article describes the first syringe pump spray pyrolysis synthesis of orthorhombic lanthanum sesquisulfide (α-La_2S_3) thin films. Two precursors lanthanum nitrate $La(NO_3)_3.6H_2O$ and thiourea ($SC(NH_2)_2$) were used to develop these rare earth chalcogenides in two different "[S]:[La]" ratios of 5 and 11. The films were developed on glass and silicon substrates. The microstructure, chemical composition, and optical properties of the (α-La_2S_3) films were thoroughly characterized using X-ray diffraction (XRD), X-ray photoelectron spectroscopy (XPS), atomic force microscopy (AFM), microanalysis, scanning electron microscopy (SEM), FTIR spectroscopy, and UV–Vis spectrometry. Microstructural analyses showed that both synthesized films had α-La_2S_3 structure and were polycrystalline. The morphology, vibration intensities, and grain sizes of the films are affected by the amount of sulfide present. The XPS results give a qualitative description of La and S as well as an indication of their potential chemical state. Measurements of particle-induced X-ray emission (PIXE) provide information on the stoichiometric ratios of the constituent components in α-La_2S_3. The optical bandgap was calculated to be 3.39 eV and 3.45 eV, respectively, for ratios 5 and 11 of the disulfide content.

Keywords α-La_2S_3 thin films · Syringe pump spray pyrolysis · Atomic force microscopy (AFM) · X-rays photoelectron spectroscopy (XPS) · Particle-induced X-ray emission (PIXE) · UV–visible and Fourier transform infrared (FTIR)

1 Introduction

In the context of increasing energy demand and environmental concerns, research has been concentrated on examining a variety of materials for energy applications and related electronics Metal/rare earth sulfides such as NiS, In_2S_3, Bi_2S_3, Ag_2S, ZnS, Gd_2S_3, and La_2S_3 have emerged as promising candidates in the field of photovoltaics, especially thin-film solar cells. Polycrystalline films of these metal/rare earth sulfides exhibit a wide variety of chemical

✉ Abdelkader Nebatti Ech-Chergui
abdelkader.nebatti@daad-alumni.de

1 Faculty of Sciences and Technology, University Belhadj Bouchaib, BP 284, 46000 Ain-Temouchent, Algeria

2 Laboratory of Theory and Simulation of Materials, Faculty of Exact and Applied Sciences, University of Oran1 Ahmed Ben Bella, Oran, Algeria

3 Department of Physics, Birla Institute of Technology, Ranchi 835215, Mesra, India

4 Unité de Physique Des Dispositifs À Semi-Conducteurs, Faculté Des Sciences de Tunis, Université de Tunis El Manar, Tunis, Tunisia

5 Laboratory of Materials (LABMAT), National Polytechnique School (ENP) of Oran, BP 1523, Oran Mnaouar, Oran, Algeria

6 Nanotechnology, Karlsruhe Institute of Technology, 76344 Eggenstein-Leopoldshafen, Germany

7 Platform of Physico-Chemical Analysis, (PTAPC-Laghouat-CRAPC), Laghouat, Algeria

8 Laboratory for Ion Beam Interactions, Ruđer Bošković Institute, Bijenička cesta 54, 10000 Zagreb, Croatia

9 Laboratory of Materials Sciences and Applications (LSMA), Faculty of Sciences and Technology, University of Ain-Temouchent Belhadj Bouchaib, Ain-Temouchent, Algeria

compositions and crystallographic phases that offer exceptionally rich and varied physicochemical properties. To determine the effectiveness of these materials in such applications, it is essential to optimize the production of these films. The lanthanum (La) reacts with sulfur (S) to form several binary compounds, including LaS (cubic), La_3S_4 (cubic), La_5S_7 (tetragonal), LaS_2 (orthorhombic), and La_2S_3 (orthorhombic) [1]. All La_2S_3 compounds can be found in either of the three crystal structures. These three crystal structures are known as the (α,β,γ-La_2S_3) phases [2]. The selected structure is influenced by many preparation factors, including the deposition temperature and thermal annealing (post-treatment). For the lighter lanthanides, the α-La_2S_3 sesquisulfide is the preferred structure, which is stable at low temperatures [3, 4]. The nearest neighbor distances are consistently more than 3 Å in this orthorhombic system with the *Pnma* space group (62) [5], which suggests that the sulfur-sulfur single bonds are uncertain. Alternatively, the nearest neighbors of the lanthanides are sulfur atoms [2]. The α-La_2S_3 phase changes into the β-La_2S_3 phase at about 1150 K with an impurity phase having the formula $La_{10}S_{14}O$. At about 1600 K, further transition into the γ-La_2S_3 phase is possible [2]. Due to its pseudocapacitive nature, the α-phase of La_2S_3 is used as an electrode when submerged in a Na_2SO_4 electrolyte in the current work [6, 7]. α-La_2S_3 has been extensively studied as a significant semiconductor material with numerous applications including rare earth alloy preparation, magnetic cooling, superconductivity, magnetic thin films, photovoltaics, pigment and thermoelectric devices, and so on. [3]. Additionally, the latter has a long history of increasing impact in science and research as a superb electrical and photonic material. Few physical deposition techniques, such as thermal evaporation [8], have been used to create thin films of (α,β,γ-La_2S_3). Chemical deposition techniques have also been used extensively, particularly atomic layer epitaxy (ALE) [9], sequential ionic adsorption and reaction method (SILAR) [10], hydrothermal microwave [11], chemical vapor deposition [12], and spray pyrolysis [3, 13, 14]. According to Patil et al. [10], who created a La_2S_3 thin film using a SILAR method, this structure is a promising electrode material for use in supercapacitors. The synthesis procedure, however, took long time. In the current work, we focus on the α-phase of La_2S_3. Spray pyrolysis was used to develop these α-La_2S_3 films. Spraying is less expensive, quicker, and offers a wider range of parameters than other chemical vapor depositions and physical vapor deposition, and it does not need a vacuum system. The spray method utilized to create La_2S_3 has received few reports of interest [3, 13, 14]. Additionally, to our knowledge, no prior study has been done on the production of α-La_2S_3 films utilizing the syringe pump spray pyrolysis (SPSP) approach from lanthanum nitrate $La(NO_3)_3.6H_2O$ and thiourea ($SC(NH_2)_2$).

2 Materials and Deposition Methods

2.1 Materials

Lanthanum nitrate La $(NO_3)_3.6H_2O$ (> 99% trace metals basis) and thiourea ($SC(NH_2)_2$ (99% purity), were supplied by Sigma-Aldrich. The chemicals were used exactly as they were obtained. No additional purification was required.

2.2 Spray Pyrolysis Setup

In this work, α-lanthanum sulfide (α-La_2S_3) films were synthesized using a syringe pump spray pyrolysis (SPSP) technique (Model No. HO-TH-04, Holmarc Ltd). It is a low-cost method for synthesizing thin films. In this method, a carrier gas and an air-atomizing nozzle are used to spray the precursor solution into tiny droplets. The experimental setup for the synthesis of α-La_2S_3 thin films is shown schematically in Fig. 1. The SPSP system is made up of four components: a PID-temperature controller, a hot plate that can reach 500 °C, a gas flow unit, and a vertically mounted infusion syringe pump that is perpendicular to the samples and has a fixed nozzle tip to substrate distance of 13 cm. The spraying head is moved in the X and Y directions under the control of a stepper. The spraying approach and deposition time were managed by a software program.

2.3 Synthesis of Lanthanum Sulfide (α-La_2S_3) Thin Films

Lanthanum nitrate $La(NO_3)_3.6H2O$ and thiourea ($SC(NH_2)_2$) were used as the base precursors for lanthanum (La) and sulfide (S), respectively, to synthesize the α-La_2S_3 phase. The molar ratio of [S]:[La] varies from 5 to 11 with the variation in the mass of thiourea from 0.12 and 0.19 M. Lanthanum's molar mass was held constant at 0.024 M. The glass substrates are 20 mm by 10 mm in size. Throughout the experiment, the deposition temperature was maintained at 300 °C, and the distance between the syringe nozzle and the substrates was maintained at 13 cm.

2.4 Film Formation Mechanism

Film formation initiates with the potential reactions that take place in the solution while synthesizing α-La_2S_3. The lanthanum ion precursor, $La(NO_3)_3$, and sulfide ion precursor,

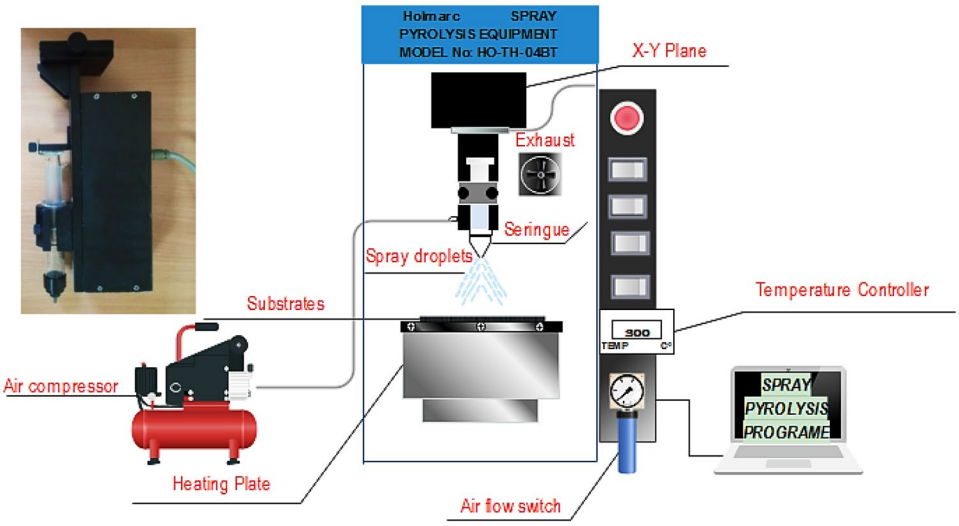

Fig. 1 Experimental setup of the lab-scale syringe spray pyrolysis (SPSP) equipment (right) and image syringe pump in operation (left)

$CS(NH_2)_2$ were dissolved to produce their respective ions. The process of lanthanum and sulfide ion production can be illustrated as follows:

$$2La(NO_3)_3 + 3CS(NH_2)_2 + 12H_2O + 6HCl \rightarrow 2La^{3+} + 6NO_3^- + 3C + 2S^{2-} + 6NH_2^- + 12H^+ + 12OH^- + 6H^+ + 6Cl^-$$

As these ions continue to interact, the molecule is created through the following chain reactions:

$2La^{3+} + 6Cl^- \rightarrow 2LaCl_3$ Formation of lanthanum chloride

$3S^{2-} + 6H^+ \rightarrow 3H_2S$ Formation of hydrogen sulfide

$6NH_2^- + 12H^+ \rightarrow 6NH_4^+$ Formation of ammonium ions

$6NO_3^- + 6NH_4^+ \rightarrow 6NH_4NO_3$ Formation of ammonium nitrate

$3C + 12OH^- \rightarrow 3C(OH)_4$ Formation of orthosilicic acid (instable component)

$3C(OH)_4 \rightarrow 3H_2CO_3 + 3H_2O$ Instant decomposition of orthosilicic acid to carbonic acid + water

Finally, the following products are formed in the reaction:

$$2La(NO_3)_3 + 3CS(NH_2)_2 + 12H_2O + 6HCl \rightarrow 2LaCl_3 + 3H_2S + 6NH_4NO_3 + 3H_2CO_3 + 3H_2O$$

These products in the solution when sprayed onto a hot substrate surface, a thermal reaction initiates between $LaCl_3$ and $3H_2S$ which result in the formation of α-La_2S_3.

About the formation of lanthanum sulfide is realized by the thermal reaction resulting from the deposition process realized by a hot substrate as the following equation:

$2LaCl_3 + 3H_2S \rightarrow La_2S_3 + 3H_2 + 3Cl_2$

2.5 Analysis Tools

The crystalline nature, structure, and phase purity of the as-synthesized α-La_2S_3 were studied by X-ray diffraction (XRD) pattern using a BRUKER D8 Advance with Cu-K_α radiation ($\lambda = 1.5406$ Å). The XRD pattern was recorded from 20 to 45° at 0.02° step size. The XPS measurements were carried out by using the "Omicron DAR 400 dual anode Mg/Al X-ray source." The Mg-K_α ($h\nu = 1253.6$ eV) excitation line was employed in this instance to record the XPS spectra, with the anode voltage and emission current set to 15 kV and 15 mA, respectively ($P = 225$ W). A Flex-Axiom Nanosurf atomic force microscope (AFM) outfitted with the potent C3000 controller was used to map the films' surface topography. The AFM pictures were processed using Gwyddion data analysis software, and the statistical values were computed in a similar manner. The optical properties of the films were studied using Perkin-Elmer Lambda 950 UV–Vis-NIR spectrometer. The PIXE analysis was carried out at Ruđer

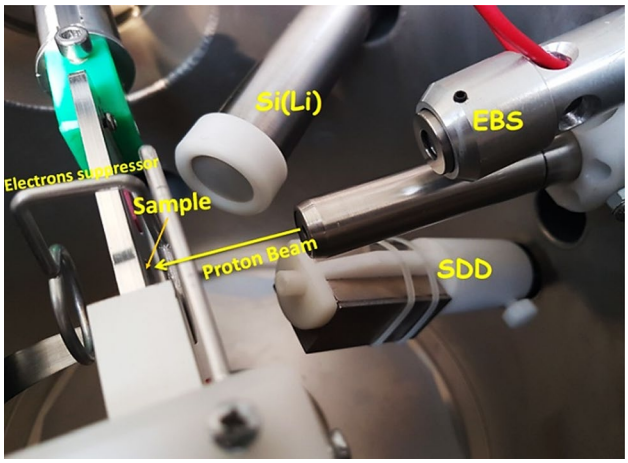

Fig. 2 Experimental setup in Standard IBA chamber for PIXE and RBS measurements

Bošković Institute in Zagreb, Croatia. In order to irradiate La_2S_3 films that had been produced on glass with a ratio of [S]:[La] = 5 and 11, a 2-MeV proton beam delivered by a 1-MV Tandetron accelerator was employed. The beam was collimated to a 3-mm diameter spot onto the target inside the vacuum chamber. Figure 2 shows the standard IBA experimental chamber. The setup primarily consists of two X-ray detectors and one surface-barrier detector used for EBS. The first X-ray detector is a silicon drift detector SDD (Vitus H20, KETEK GmbH) placed at 150° to the incident beam with 10 mm^2 active area and 8-µm thin Be window, this detector is used for low-energy range.

The second X-ray detector is Si(Li) detector at 135° (SSL80165, Canberra) with a 30 mm^2 active area and 25-µm Be window thickness, 275 Mylar filter is placed in front of the detector to absorb low-energy X-rays which makes this detector more efficient for detection of X-ray lines above 3.5 keV. The energy spectrum was collected through a signal processing chain and final data were analyzed using GUPIXWIN software.

3 Results and Discussion

3.1 X-Ray Diffraction (XRD) Analysis

Figure 3 displays the X-ray diffraction patterns of lanthanum sulfide films with two molar ratios [S]:[La] = 5 and 11 that were recorded in the 2θ range of 20–45°. Both synthesized films were found to be polycrystalline and showed multiple peaks corresponding to (200), (111), (112), (203), (105), (204), and (115) planes. These planes closely matched the JCPDS card No: c73-957 and C71-2349, which are indicative of α-La_2S_3 with an orthorhombic lattice and a space group (*Pnma*). The calculated lattice parameters are a = 7.66 Å, b = 4.22 Å, c =15.95 Å. A variety of preferred orientations were revealed by the relative intensities of the indicated

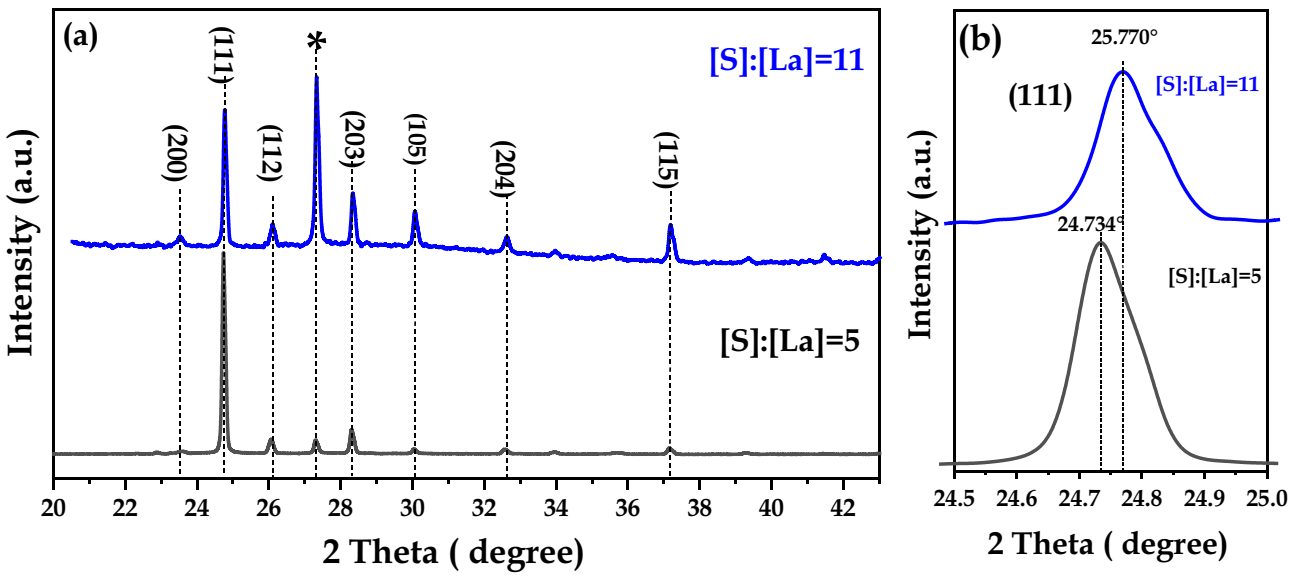

Fig. 3 **a** X-ray diffraction patterns of α-La_2S_3 thin films with various [S]:[La] ratios. **b** Enlarged spectra of 2 theta from 24 to 25.6 degree. The asterisks (*) mark the peaks (LaS_2 phase)

peaks, which varied significantly from sample to sample. The diffraction patterns showed no evidence of lanthanum oxysulfide or other oxide phases, such as La_2O_3 or La-S–O ternaries.

One of the peaks in the diffraction profile remains unindexed and is indicated by the asterisk mark "*." This reflection at $2\theta = 27.2°$ corresponds to the LaS_2 phase. The peak intensity of the LaS_2 phase and (α-La_2S_3) is significantly influenced by sulfide content. In the film with [S]:[La] ratio 5, the peak intensity of the LaS_2 phase decreases, and the strongest diffraction intensity is seen along the (111) plane, suggesting that the sample had a better-preferred synthesis. Figure 3b reveals that as the mass ratio increases, the diffraction peak corresponding to the (111) plane move slightly to higher angles, indicating a reduction in the crystalline lattice spacing (d) of α-La_2S_3. This was probably due to the sulfide concentration. The average crystallite size D of α-La_2S_3 films was calculated with the help of Scherrer's formula [15]

$$D_{(hkl)} = \frac{K\lambda}{\beta_{(hkl)} \cos \theta_{(hkl)}}$$

where λ (1.5406 Å for Cu (Kα)) corresponds to the wavelength of the X-ray, θ is the diffraction angle, and β is the full width of the diffraction peak at half of its maximum intensity. For ratios 5 and 11, it was determined that the crystallite size of α-La_2S_3 films for the (111) plane was 51.43 nm and 34.88 nm, respectively. Similar values of roughly 46 nm were obtained by Patil et al. [10] for α-La_2S_3 films produced by the SILAR technique.

3.2 Atomic Force Microscopy (AFM) Microanalysis

Surface roughness is an important parameter since it gives information about the morphology of the deposit. Roughness can only be determined using statistical elements. The roughness was examined in terms of RMS (root mean square) parameter, which represents the standard deviation, as shown in the following equation [16]:

$$RMS = \sqrt{\left(\frac{\sum_{i=1}^{512} \sum_{j=1}^{512} h_{ij}^2}{512^2} - \langle \eta \rangle^2 \right)}$$

where i and j denoted the number of points that make up the image, i.e., the number of pixels (in our case $i = j = 512$) and $\langle \eta \rangle$, the value of the average height of the distributions h_{ij}.

Figure 4 shows the AFM images of both α-La_2S_3 films with the ratio of 5 and 11. These surface topographies show that the surface consists of grains that grew perpendicularly. It also shows that the surface of the sample with a ratio of 5 has higher porosity. It is worth noting that the higher RMS value denotes a very porous surface. The RMS values are estimated to be 82.5 nm and 47.5 nm, respectively, for the films with ratios 5 and 11. The film having ratio 11 has larger grains than the film having ratio 5, suggesting stronger coalescence in the respective film.

The grain size of the films were quantified using a self-correlation function G, defined by the following equation [17]

$$G(k_1, k_2) = \sum_{i=1}^{512} \sum_{j=1}^{512} h(i,j) \times h(i + k_1, j + k_2)$$

where $h(i,j)$ is the height of the film at the point of coordinates (i,j). Figure 5 shows a profile section of the central spot of the self-correlation images used to determine the grain size of the films. The typical grain size is shown by a peak whose breadth is half its height. Film with molar ratio 5 shows grains of the average size of 100 nm (dx = 100 nm along the X axis and dy = 105 nm along the Y axis). These grains form spherical islands. These values are similar

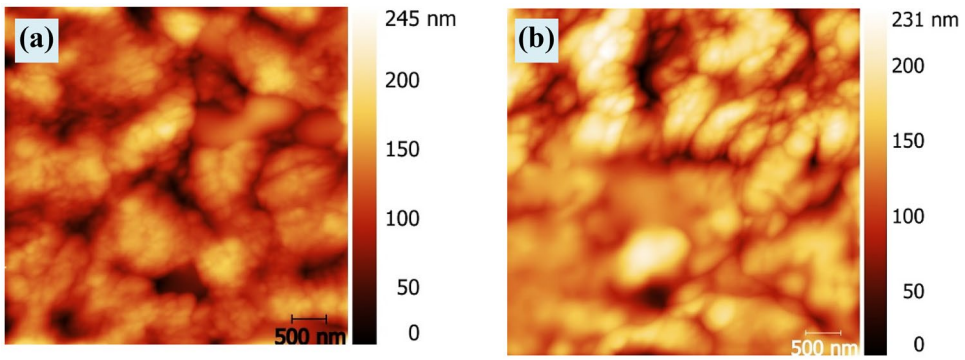

Fig. 4 2D AFM images (5 µm × 5 µm and in tapping mode) of α-La_2S_3 with two ratios: **a** [S]:[La] = 5, **b** [S]:[La] = 11

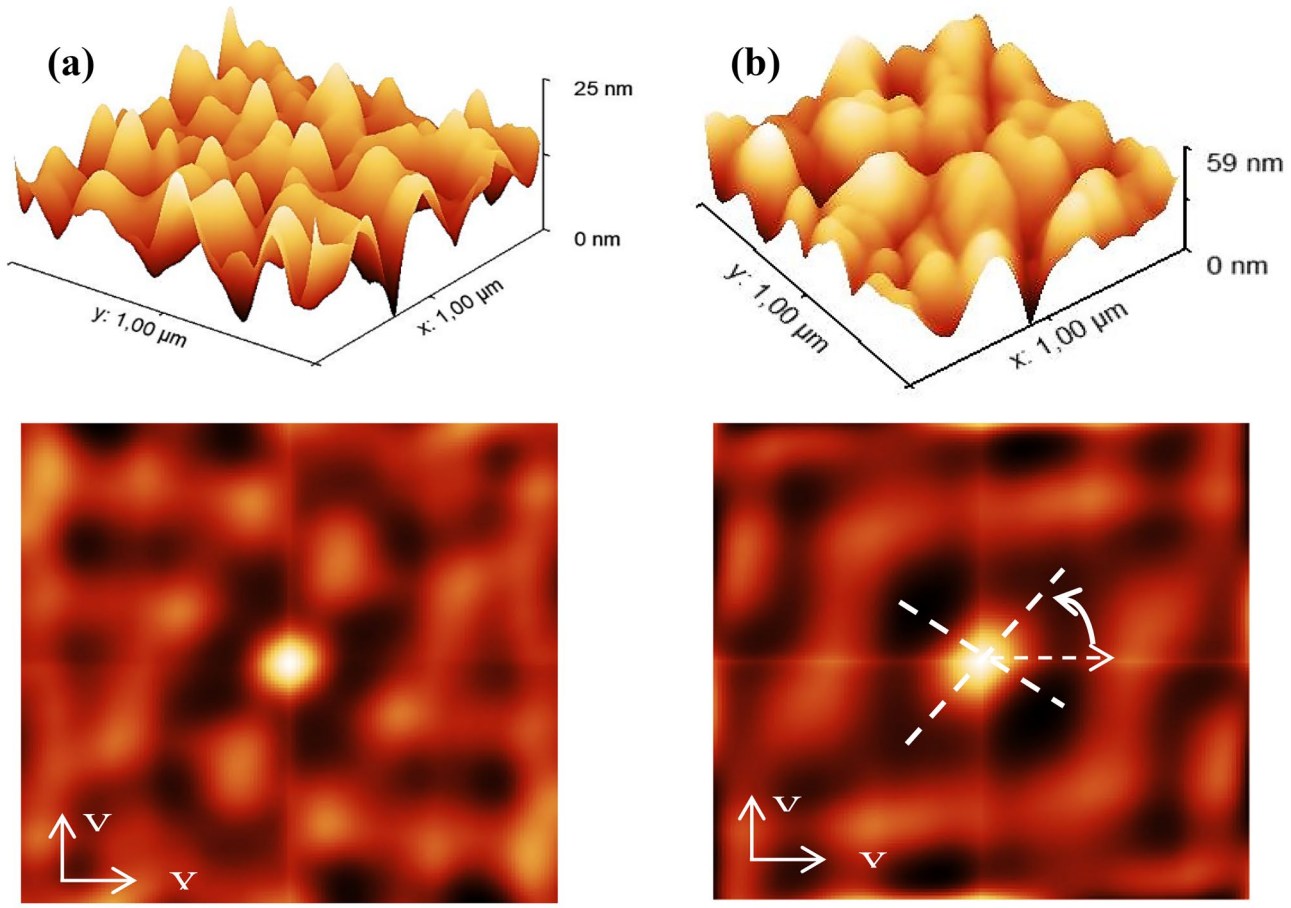

Fig. 5 3D-AFM images with self-correlation images (1 µm × 1 µm) of α-La_2S_3 films having molar ratio: **a** [S]:[La] = 5, **b** [S]:[La] = 11

to those for Cu_xS layers in the literature [18]. According to the self-correlation picture, the film with ratio 11 (dx = 111.5 nm along the X axis and dy = 134.5 nm along the Y axis) is made up of bigger, elongated grains. This is because when the layer grows, there is a strong coalescence between the grains, which causes them to overlap. This phenomenon explains how a thin film produces a layer with less porosity.

3.3 Chemical Composition Analysis

3.3.1 X-Ray Photoelectron Spectroscopy XPS of Untreated and Treated Surfaces

The surface chemical composition of the synthesized films was characterized using XPS analysis before (as-deposited films) and after Ar ion sputtering treatment (cleaned films). The treatment process was realized as described by Bouslama et al. [19]. The purpose was to remove the contamination layers forming during air exposure of La_2S_3 films. The as-deposited α-La_2S_3 film with ratio of [S]:[La] = 5 was selected for the XPS measurement required to study their chemical composition. The XPS survey spectra of α-La_2S_3 surfaces are shown in Fig. 6a. The core-level photoelectron peaks (doubled La 3d, O 1 s, S 2 s, La 4d, La 5 s, and La 5p) and Auger transition ones (La MNN and O KLL) related to La_2S_3 compound are well identified. Besides, the significant reduction of C 1s and C KLL signals corresponding to adventitious carbon shown after treatment indicates that the surface is fairly clean. In addition, Fig. 6b, c show the high-resolution XPS spectra of cleaned α-La_2S_3 film corresponding to doubled La 3d (La $3d_{3/2}$ and La$3d_{5/2}$) and S 2p core-levels peaks, respectively. Figure 6b displays a main peak of La $3d_{5/2}$ at 838.4 eV attributed to La^{3+} ions accompanied by a shoulder at 835.0 eV due to La^0

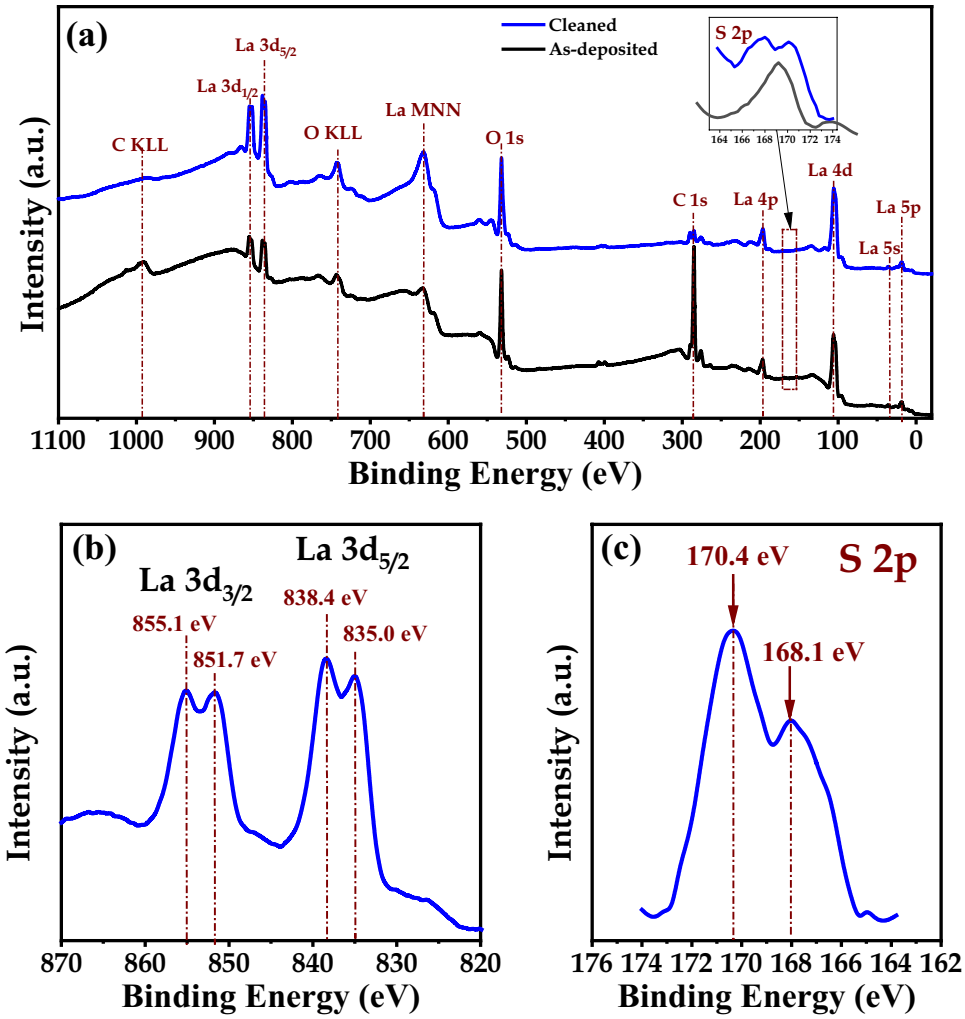

Fig. 6 XPS spectra of α-La_2S_3 films (with ratio of [S]:[La] = 5) recorded before (As-deposited) after Ar ion sputtering treatment (cleaned) using Mg-Kα (hν = 1253.6 eV) excitation line. **a** Survey spectra. **b** and **c** High-resolution spectra of doubled La 3d and S 2p core-level peaks corresponding to cleaned α-La_2S_3 films

bonds [20]. On the other hand, Fig. 6c displays a main peak at 170.4 eV due to the overlapping between S $2p_{1/2}$ and S $2p_{3/2}$ and attributed to the SO_3 group accompanied by a shoulder at 168.1eV due to S 2p of S^{2-} in La-S bonds [20].

3.3.2 PIXE Analysis

Particle-induced X-ray emission (PIXE) measurements were performed to examine the elemental composition of our samples along with other contaminations. The typical X-ray spectra recorded for La_2S_3 samples are shown in Fig. 5. Only data from the SDD detector were analyzed because of the low-energy range of both elements to be quantified (Kα (S) = 2.3 keV and Lα (La) = 4.6 keV). The PIXE spectrum shows peaks corresponding to the X-rays emitted by substrate and deposited film elements. It can be observed from X-ray line intensities of elements present in the sample that these are distributed according to their stoichiometric ratios. Integral intensity of La-Lα for [S]:[La] = 5 is higher than [S]:[La] = 11 while S-Kα for [S]:[La] = 5 is lower than [S]:[La] = 11. Since the PIXE spectrum has SDD detector, the X-ray lines of La element is detected over by even Lγ2.

Furthermore, traces Na, Ca, Fe, and Cu are also observed as X-ray lines in PIXE spectra due to surface contamination of either substrate or impurities present in the solutions. The elemental concentration of La and

Table 1 Measured concentration of S and La in ppm using PIXE technique

Sample	S (ppm)	La (ppm)
[S]: [La] = 5	4211	536,012.9
[S]: [La] = 11	7412.7	374,662.2

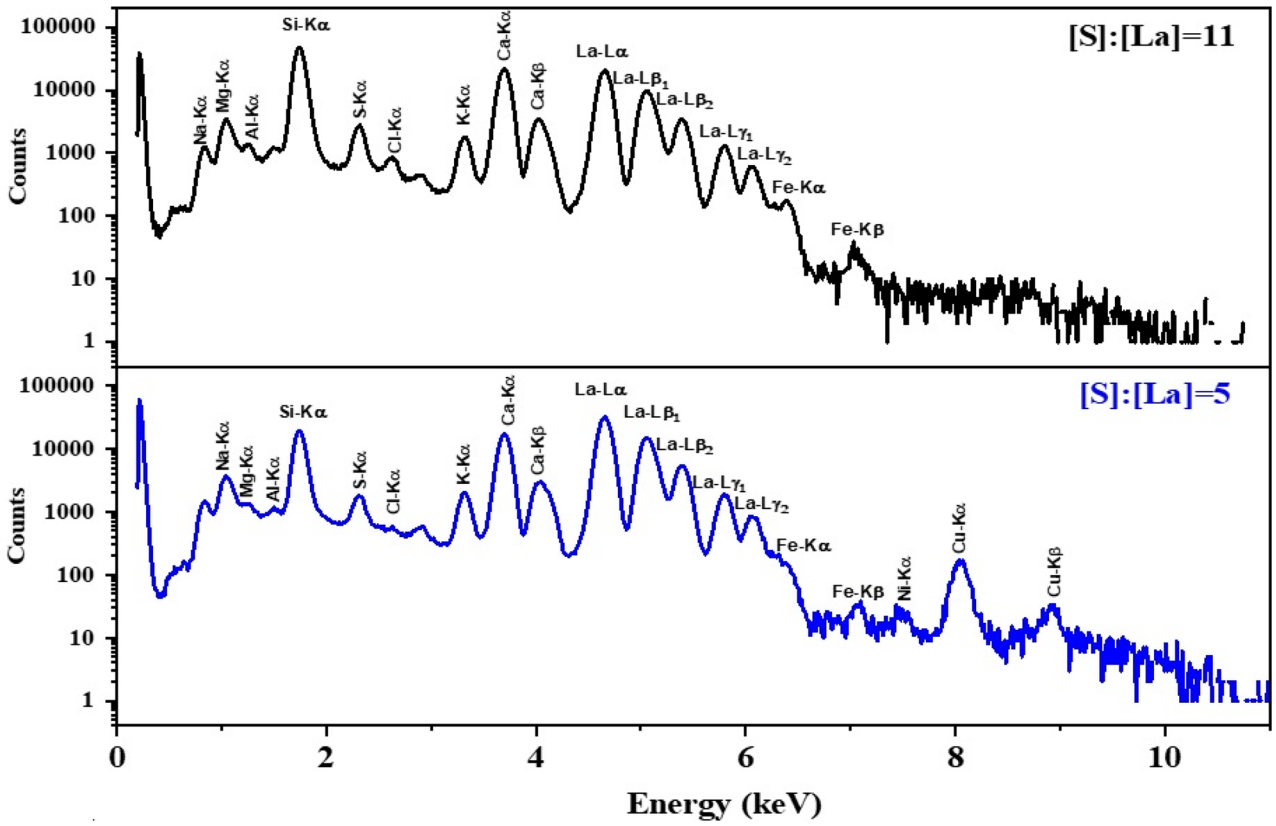

Fig. 7 Typical PIXE spectra of La_2S_3 film deposited on glass with ratio [S]:[La] = 5 and 11

S in La_2S_3 films in terms of ppm (parts per million) is presented in Table 1. Validation of the method was done by analyzing NIST 620 certified reference standard, the measured value is in good agreement with the certified value (Fig. 7).

3.4 FTIR Spectroscopy Analysis

Figure 8 displays the FTIR spectra of α-La_2S_3 films produced by spray pyrolysis with two ratios of [S]:[La] = 5 and 11. The analysis was done to identify the functional groups in the films. The FTIR spectrum shows several transmission peaks at 597.26 cm^{-1} (metal sulfide La-S), 839 cm^{-1} (La_2S_3 with adsorbed SO_3^{2-}), a small band in the range of 3200–3631.27 cm^{-1} which is an indicative of the O–H stretching vibration, and a band with a center at 1636 cm^{-1} which denotes a distinctive H–O-H bending vibration mode [21, 22]. Furthermore, the strongest band in the spectrum at 597.26 cm^{-1} corresponds to sulfide compounds possibly due to stretching vibrations of La_2S_3. The peaks between 500 and 650 cm^{-1} are attributed to the metal-sulfur vibrations, according to Kim and co-workers [24].

Consequently, the FTIR spectrum shown in Fig. 6 is consistent with the La_2S_3 spectrum that was previously characterized by Rashidi Nodeh et al. [22]. It should be noted that the peak positions in the spectra were unaffected by the molar ratio. However, as the ratio was reduced from 11 to 5, the intensity of vibrations decreased, indicating that there was more functional group present in the film. A band in the region 490–689 cm^{-1} that is an indicative of La-S stretching vibrations [21], became narrower with increasing sulfide content. Finally, the films also contained some carbon-related species, as evidenced by the bands centered at 1020 cm^{-1} corresponding to C-O vibration [23].

3.5 Optical Characterization of the α-La_2S_3 Thin Films

The transmission spectra for α-La_2S_3 films with ratios 5 and 11 are shown in Fig. 9a, c. Optical characterization of the films was done to explore the relationship between the band gap energy of synthesized films and the sulfide content. The transmission spectra of the films were measured between the wavelengths of 300 and 1000 nm.

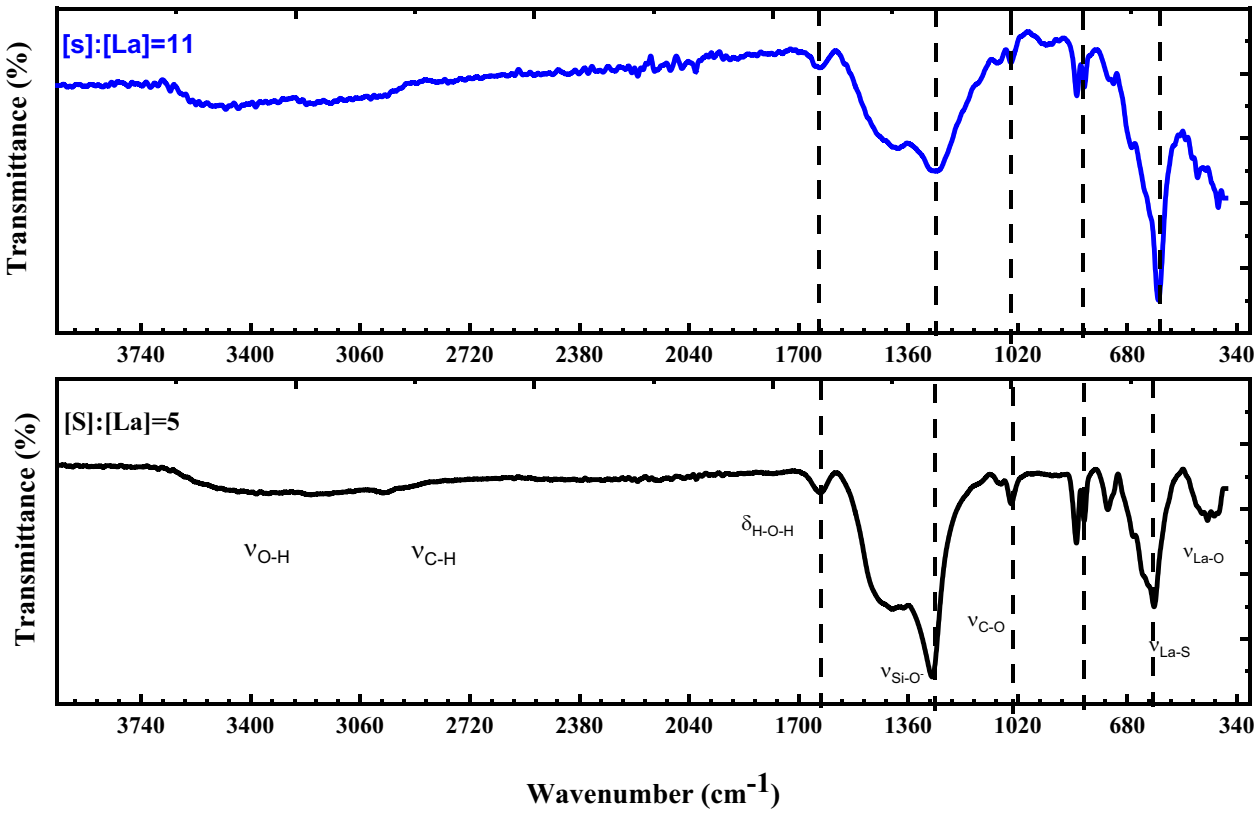

Fig. 8 FTIR spectrum of La_2S_3 thin films on glass substrate synthesized by spray pyrolysis with two ratios [S]:[La] = 5 and 11

The transparency of both the films is high, about 65% in the 600–100-nm range. Remarkably, neither spectrum showed the phenomena of interference fringe patterns in transmission, certainly because of higher thickness and homogeneity, which can contribute too much scattering/absorption in the film [24, 25]. It can be seen in Fig. 9b, d (Tauc plots), as the sulfide content increased (from ratio 5 to ratio 11), the absorption edge (380 nm) shifted toward the lower wavelength range. The band gap energy (E_g) could be predicted from the optical transmission spectra by calculating the absorption coefficient using the Tauc equation

$$(\alpha\, h\nu)^2 = A\left(h\nu - E_g\right)$$

where α is photo-absorption coefficient, h is Plank's constant, ν is the photon frequency, and E_g is the energy band gap of film (eV). The variation of $(\alpha h\nu)^2$ with photon energy $h\nu$ for both ratio 5 and 11 α-La_2S_3 films is shown in Fig. 9b, d. It has been observed that the plots of $(\alpha h\nu)^2$ versus $h\nu$ are nearly linear over a wide range of photon energies indicating the direct type of transitions. The intercepts (extrapolations) of these plots (straight lines) on the energy axis ($\alpha = 0$) give the energy band gaps from the plot; the energy band gap was expected to be $E_g = 3.39$ and 3.45 eV for ratios 5 and 11, respectively. This was significantly higher than that reported by Biswas and Varadaraju [26] and Bagde et al. [3]. This could be due to the deposition process and precursors used. Yan-chao et al. [27], Marin et al. [28], Zhang et al. [11], and Coussens [29] indicate that the lanthanide sulfides have band gaps of 2.5 eV or higher up to 4.02 eV. Our results are comparable to those reported in the literature and for La_2S_3 thin films synthesized using a liquid-phase approach, which exhibit a wide band gap [28].

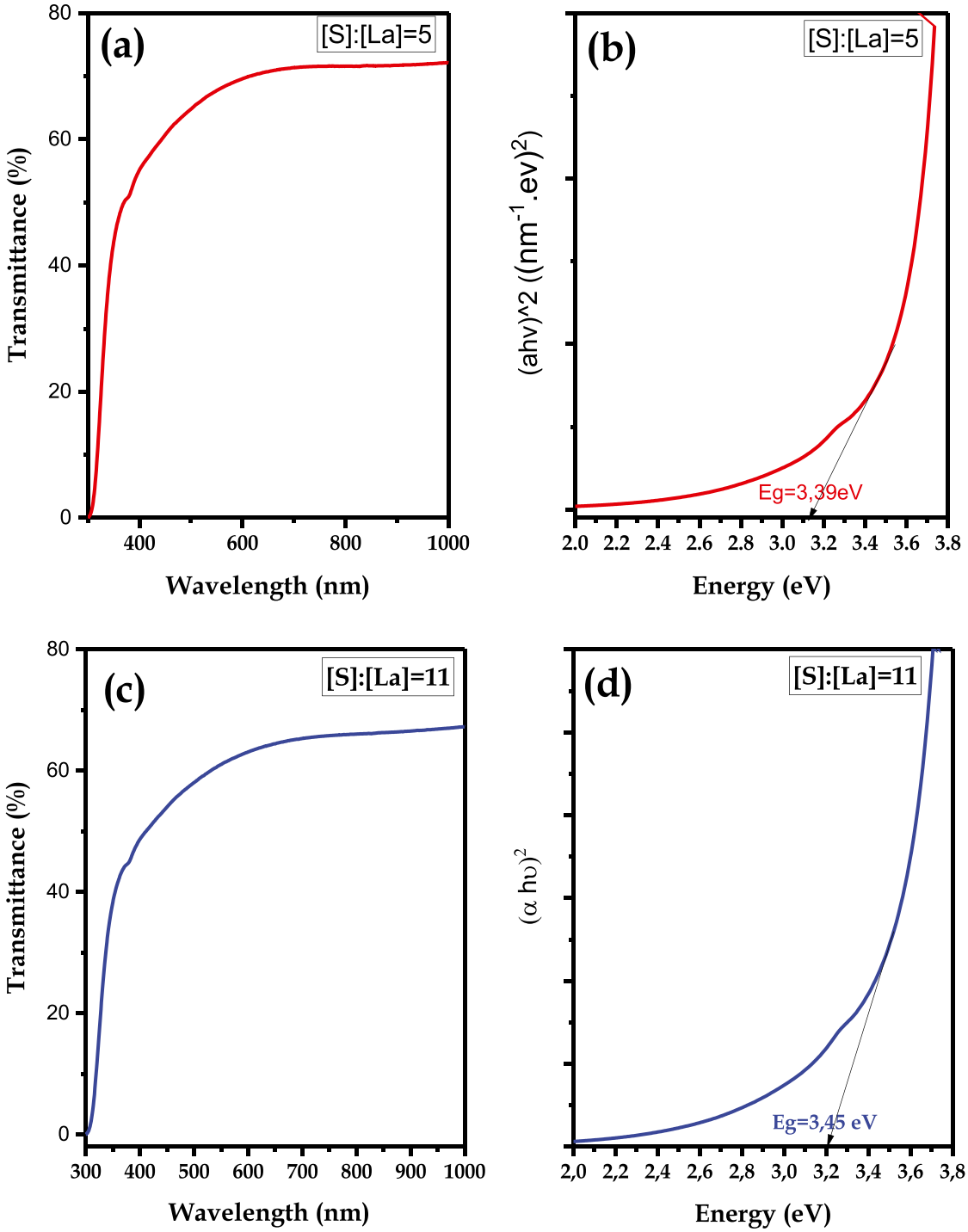

Fig. 9 The transmittance spectra and the Tauc plot of α-La_2S_3 films with two ratio **a** [S]:[La] = 5 and **b** [S]:[La] = 11

4 Conclusion

The current study demonstrates a novel syringe pump spray pyrolysis (SPSP) method for producing orthorhombic α-La_2S_3 from two precursors, lanthanum nitrate $La(NO_3)_3.6H_2O$, and thiourea ($SC(NH_2)_2$). The structural analysis indicates polycrystalline orthorhombic La_2S_3 films in the α-phase. Films with high molar ratio [S]:[La] = 11 also evidenced a sulfide phase (LaS_2) in it. The formation of La_2S_3 was also verified by XPS and FTIR. The presence of La and S in stochiometric ratios in the La_2S_3 films was confirmed by PIXE measurements. AFM images showed that the grain size

increased as the sulfide concentration increased. The band gap increased from 3.39 to 3.45 eV with a rise in sulfide content. With the increase of sulfide concentration, the band gap increased from 3.39 to 3.45 eV for ratio 5 and ratio 11 respectively (as shown by UV–visible). However, the transmittance decreases slightly. Overall, this approach can be used as a promising low-cost system for synthesizing thin films.

Acknowledgements The authors are grateful to the Laboratory of Theory and Simulation of Materials (LTSM) Facility for support and access to spray machine.

Declarations

Conflict of Interest The authors declare no competing interests.

References

1. P.N. Kumta, S.H. Risbud, Chemical processing of rare earth chalcogenides. Prog. Cryst. Growth Charact. Mater. **22**, 321–383 (1991)
2. C. Marin, Synthesis and applications of lanthanide sulfides and oxides. (2016)
3. G. Bagde, H. Pathan, C. Lokhande, S. Patil, M. Muller, Studies on sprayed lanthanum sulphide (La_2S_3) thin films from non-aqueous medium. Appl. Surf. Sci. **252**, 1502–1509 (2005)
4. M. Ohta, S. Hirai, H. Asahi, T. Nishimura, Y. Uemura, K. Shimakage, Synthesis of La_2S_3 thin films by sulfurization of $LaCl_3$ and CS (NH_2) 2. Mater. Trans. **47**, 1436–1439 (2006)
5. Y. Yang, C. Mi, F. Jiao, X. Su, X. Li, L. Liu, J. Zhang, F. Yu, Y. Liu, Y. Mai, A novel multifunctional upconversion phosphor: Yb^{3+}/Er^{3+} codoped La_2S_3. J. Am. Ceram. Soc. **97**, 1769–1775 (2014)
6. S. Patil, A. Lokhande, C. Lokhande, Effect of aqueous electrolyte on pseudocapacitive behavior of chemically synthesized La_2S_3 electrode. Mater. Sci. Semicond. Process. **41**, 132–136 (2016)
7. M. Isobe, A. Hayashi, Y. Ueda, Preparation and some physical properties of superconducting $La_{3-x}S_4$ and $La_{3-y}Ba_yS_4$. Physica C **235**, 777–778 (1994)
8. D. Berkeley, J. Kang, J. Maps, J.-C. Wan, A. Goldman, Vapor-deposited superconducting lanthanum sulfide films. Thin Solid Films **156**, 271–276 (1988)
9. K. Kukli, H. Heikkinen, E. Nykänen, L. Niinistö, Deposition of lanthanum sulfide thin films by atomic layer epitaxy. J. Alloy. Compd. **275**, 10–14 (1998)
10. S. Patil, V. Kumbhar, B. Patil, R. Bulakhe, C. Lokhande, Chemical synthesis of α-La_2S_3 thin film as an advanced electrode material for supercapacitor application. J. Alloy. Compd. **611**, 191–196 (2014)
11. Y. Zhang, L.Y. Cao, J.F. Huang, J.P. Wu, Influence of S/La molar ratio on the morphology and optical property of La_2S_3 microcrystalline prepared by microwave hydrothermal. Key Eng. Mater. **512-515**, Trans. Tech. Publ. 223–226 (2012)
12. L. Tian, T. Ouyang, K.P. Loh, J.J. Vittal, La_2S_3 thin films from metal organic chemical vapor deposition of single-source precursor. J. Mater. Chem. **16**, 272–277 (2006)
13. G. Bagde, S. Sartale, C. Lokhande, Deposition and annealing effect on lanthanum sulfide thin films by spray pyrolysis. Thin Solid Films **445**, 1–6 (2003)
14. G. Bagde, C. Londhe, A. Bagde, Morphological studies on spray deposited lanthanum sulphide (La_2S_3) thin films. Key Eng. Mater. **705** Trans. Tech. Publ. 283–288 (2016)
15. B. D. Cullity, Elements of x-ray diffraction, Addison-Wesley Publishing Co, Reading, MA. **102** (1978)
16. N. Benaioun, I. Maafa, A. Florentin, E. Denys, N. Hakiki, N. Moulayat, J. Bubendorff, Time dependence of the natural passivation process on AISI 304 in an alkaline medium: Atomic force microscopy and scanning Kelvin probe force microscopy as additional tools to electrochemical impedance spectroscopy. Appl. Surf. Sci. **436**, 646–652 (2018)
17. F. Mechehoud, N. Benaioun, N. Hakiki, A. Khelil, L. Simon, J.-L. Bubendorff, Thermally oxidized Inconel 600 and 690 nickel-based alloys characterizations by combination of global photoelectrochemistry and local near-field microscopy techniques (STM, STS, AFM, SKPFM). Appl. Surf. Sci. **433**, 66–75 (2018)
18. L. Reijnen, B. Meester, A. Goossens, J. Schoonman, Atomic layer deposition of Cu_xS for solar energy conversion. Chem. Vap. Deposition **9**, 15–20 (2003)
19. M.H. Bouslama, A. Ouerdane, A. Mokadem, B. Kharroubi, M. Bedrouni, M. Abdelkrim, A. Abdellaoui, K.B. Bensassi, A. Baizid, M.S. Halati, Chemical, morphological and optical properties of undoped and Cu-doped ZnO thin films submitted to UHV treatment. Appl. Surf. Sci. **520**, 146302 (2020)
20. J. Chastain, R.C. King Jr., Handbook of X-ray photoelectron spectroscopy. Perkin-Elmer Corporation **40**, 221 (1992)
21. B.J. Tsay, L.H. Wang, A study on infrared transmission of lanthanum sulfide and oxysulfide in the 2.5–14 μm region. Mater. Lett. **34**, 180–183 (1998)
22. H. Rashidi Nodeh, H. Sereshti, E. Beirakabadi, K. Razmkhah, Synthesis and application of lanthanum sulfide nanoparticles for removal of tetracycline from aqueous media. Int. J. Environ. Sci. Technol. **17**, 819–828 (2020)
23. B.J. Cha, S. Saqlain, H.O. Seo, Y.D. Kim, Hydrophilic surface modification of TiO_2 to produce a highly sustainable photocatalyst for outdoor air purification. Appl. Surf. Sci. **479**, 31–38 (2019)
24. M. Caglar, Y. Caglar, S. Ilican, The determination of the thickness and optical constants of the ZnO crystalline thin film by using envelope method. J. Optoelectron. Adv. Mater. **8**, 1410 (2006)
25. J. Klein, A. Yen, S. Cogan, Determining thin film properties by fitting optical transmittance. J. Appl. Phys. **68**, 1825–1830 (1990)
26. K. Biswas, U. Varadaraju, Stabilization of γ-La_2S_3 by alkali metal ion doping. Mater. Res. Bull. **42**, 385–388 (2007)
27. H. Yan-chao, H. Jian-feng, Z. Xuan, C. Li-yun, Y. Li-Xiong, Preparation of Sm_2S_3 thin films by liquid phase deposition method with self-assembled monolayers. J. Alloy. Compd. **536**, 119–123 (2012)
28. C.M. Marin, L. Wang, J.R. Brewer, W.-N. Mei, C.L. Cheung, Crystalline α-Sm_2S_3 nanowires: Structure and optical properties of an unusual intrinsically degenerate semiconductor. J. Alloy. Compd. **563**, 293–299 (2013)
29. N.J. Coussens, Lanthanum sulfide thin film deposition via chemical nanocluster deposition. Honors College Thesis, Oregon State University (2009)